ACS Sustainable Chemistry & Engineering

pubs.acs.org/journal/ascecg

Research Article

Phase Equilibria and Diffusivities of HFC-32 and HFC-125 in Ionic Liquids for the Separation of R-410A

Kalin R. Baca, Greta M. Olsen, Lucia Matamoros Valenciano, Madelyn G. Bennett, Dorothy M. Haggard, Bridgette J. Befort, Alejandro Garciadiego, Alexander W. Dowling, Edward J. Maginn, and Mark B. Shiflett*

Cite This: *ACS Sustainable Chem. Eng.* 2022, 10, 816−830

Read Online

ACCESS | Metrics & More | Article Recommendations | Supporting Information

ABSTRACT: Current legislation calling for the phase out of hydrofluorocarbon (HFC) refrigerants is driving a global market shift that has prompted industry and research institutions to investigate new refrigerant mixtures and sustainable separation techniques for recycling refrigerants. The recent American Innovation and Manufacturing (AIM) Act of 2020 requires an 85% phase down of HFC production over the next 15 years. To achieve this goal, azeotropic refrigerant mixtures, such as R-410A composed of 50 wt % HFC-32 (difluoromethane, CH_2F_2) and 50 wt % HFC-125 (pentafluoroethane, CHF_2CF_3), will have to be separated to recycle the lower global warming HFC-32 component. The present work investigates the solubility of HFC-32 and HFC-125 in six ionic liquids (ILs) with halogen anions for the purpose of developing the thermophysical property data required for designing extractive distillation recycling processes and understanding the choice of cation and anion type. A gravimetric microbalance was used to collect isothermal vapor liquid equilibrium data for each of the ILs at 298.15 K and pressures from 0.05 to 1.0 MPa. The Peng−Robinson equation of state was used to model the solubility of the HFCs in the ILs. The solubility of HFC-32 in the ILs showed small differences, while the solubility of HFC-125 had significant variations with respect to the anion type and the cation alkyl chain length. Fick's law was applied to calculate diffusion coefficients for each HFC/IL system. HFC-32 has a greater diffusivity than HFC-125 based on smaller molecular size. The 1-*n*-hexyl-3-methylimidazolium chloride and the trihexyl(tetradecyl)-phosphonium chloride ILs have the highest HFC-125/HFC-32 selectivity at 298.15 K. Based on both the mass uptake and selectivity ratio, these two ILs are potential entrainers for the separation of R-410A using extractive distillation.

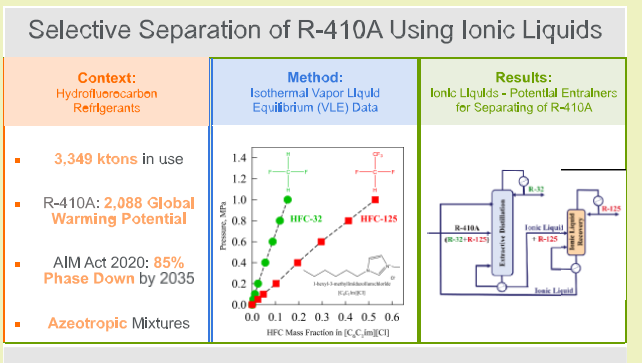

KEYWORDS: *hydrofluorocarbons, refrigerants, ionic liquids, phase equilibria, and separation*

1. INTRODUCTION

The global refrigerant market is rapidly growing and is currently valued at $14 billion annually. The total amount of refrigerant in use is 3349 ktons, and 2833 ktons are used in applications with fugitive emissions.[1] These applications include vapor compression, fire suppression, foam production, aerosols, solvents, and chemical production.[1] Fluorocarbon refrigerants make up 44% of the total refrigerant market, and vapor compression systems are the "most difficult and impactful area for refrigerant innovation".[1] Chlorofluorocarbon (CFC) refrigerants, which are non-flammable and non-toxic, were invented in the early 1930s as safe alternatives to ammonia, methyl chloride, and sulfur dioxide. CFCs had a tremendous impact on the rapid development of the refrigeration and air-conditioning (RAC) industry. Their unintended impact on the environment, however, has led to a global phase out agreements and regulations.

In 1987, the Montreal Protocol phased out both the production and use of CFCs, and subsequently hydrochlorofluorocarbons (HCFCs) due to high ozone depletion potentials.[3,4] Hydrofluorocarbon (HFC) refrigerants were developed in the 1990s to replace CFCs and HCFCs and are widely used today in a variety of RAC applications. HFCs have excellent refrigerant properties and zero ozone depletion potential; however, due to their high global warming potential (GWP), HFCs are being phased down, see Figure 1.[3] The recent American Innovation and Manufacturing (AIM) Act of

Received: September 12, 2021
Revised: November 13, 2021
Published: December 3, 2021

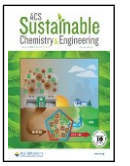

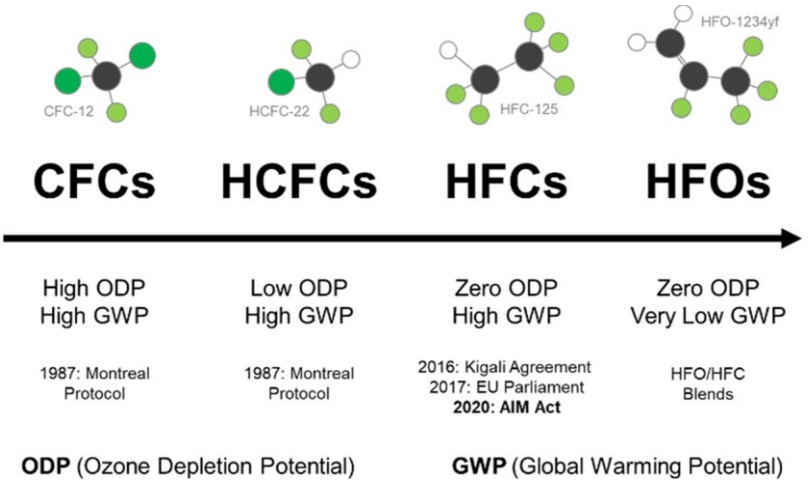

Figure 1. Fluorocarbon refrigerant generations, environmental impact, and the corresponding legislation.[2]

Table 1. ILs' Physical Properties[17,18]

ionic liquid	formula	MW (g·mol^{-1})	melting point (K)	density (kg·m^{-3})	viscosity (Pa·s)
[C_6C_1im][I]	$C_{10}H_{19}IN_2$	294.18	<RT	1384.09 ± 0.96[19]	1.8 ± 0.2[20]
[C_6C_1im][Br]	$C_{10}H_{19}BrN_2$	247.18	<RT	1228.17 ± 0.69[21]	3.6 ± 0.8[22]
[C_6C_1im][Cl]	$C_{10}H_{19}ClN_2$	202.72	<RT	1039.7 ± 2.7[23]	18.1 ± 1.8[15,23]
[C_4C_1im][Cl]	$C_8H_{15}ClN_2$	174.67	338.15−343.5[24,25]	1074 ± 10[26]	
[C_3C_1im][Cl]	$C_7H_{13}ClN_2$	160.65	333.15[27]	1109.11 ± 0.44[28]	
[C_2C_1im][Cl]	$C_6H_{11}ClN_2$	146.62	350.15−360.15[29,30]	1143.4 ± 1.2[28]	
[$P_{6,6,6,14}$][Cl]	$C_{32}H_{68}ClP$	519.32	<RT	892.80 ± 6.2[31]	1.68 ± 0.25[31]

2020 proposed an 85% phase down of both production and consumption of HFCs by 2035.[5,6] This moves up the phase out timeline proposed by the Kigali Amendment to the Montreal Protocol by nearly 10 years and is comparable to the Regulation EU 517/2014 in Europe.[3,7] It is imperative for the successful phase out of HFCs that the next generation (i.e., fourth generation) of refrigerants known as hydrofluoroolefins (HFOs) and blends of HFCs with HFOs are available for broad adoption across the RAC industry.[1,4]

The phase out of millions of tons of HFC refrigerants provides a tremendous need to separate and recycle high GWP HFC refrigerant mixtures.[3,8] Common HFC refrigerant mixtures include R-404A, R-507, R-407A, R-407C, and R-410A, all of which are composed of various combinations and amounts of HFC-125, HFC-32, 1,1,1-trifluoroethane (HFC-143a, CH_3CF_3), and 1,1,1,2-tetrafluoroethane (HFC-134a, CH_2FCF_3); see Table S1 in the Supporting Information for details.[1,9,10] The separation of these azeotropic and near-azeotropic mixtures is difficult to impossible using conventional distillation techniques. For this reason, research is needed to develop separation techniques such as extractive distillation, pressure-swing adsorption (PSA), and membrane processes for breaking the azeotropic compositions to produce pure refrigerants. Ionic liquids (ILs) are ideal entrainers for extractive distillation because ILs have essentially no measurable vapor pressure (i.e., $<1 \times 10^{-3}$ to 1×10^{-5} Pa) and will not contaminate the product streams.[11−14] This study is a continuation of research focused on experimental measurements and modeling to identify IL-based entrainers for the separation of R-410A. R-410A is a near azeotropic refrigerant mixture composed of 50 wt % HFC-32 and 50 wt % HFC-125. R-410A is the most widely used refrigerant blend for air-conditioning applications, and regulations phasing down this refrigerant mixture will have a significant impact on the RAC industry.[1]

Morais et al. investigated the solubility and diffusivity of HFC-32 and HFC-125 in six different ILs, three with fluorinated anions and three with non-fluorinated anions.[15] The study confirmed that HFC-32 was more soluble in ILs containing fluorinated anions,[15] and recent molecular modeling indicates that the hydrogens on CH_2F_2 strongly interact with fluorines on the anions (e.g., PF_6^- and BF_4^-). Morais et al. also found that HFC-125 was more soluble in ILs with non-fluorinated anions,[15] and molecular modeling shows that the hydrogens on the cation alkyl chains strongly interact with fluorines on CHF_2CF_3 in the absence of a fluorinated anion. One of the most promising ILs identified in that study was 1-*n*-hexyl-3-methylimidazolium chloride ([C_6C_1im][Cl]), which showed a large difference in mass fraction solubility between HFC-32 and HFC-125, suggesting that this IL could be used as an entrainer for extractive distillation to separate R-410A.[15] The current work continues the investigation of HFC-32 and HFC-125 solubility in six new ILs with halogen anions: 1-*n*-hexyl-3-methylimidazolium iodide [C_6C_1im][I], 1-*n*-hexyl-3-methylimidazolium bromide [C_6C_1im][Br], 1-*n*-butyl-3-methylimidazolium chloride [C_4C_1im][Cl], 1-methyl-3-propylimidazolium chloride [C_3C_1im][Cl], 1-ethyl-3-methylimidazolium chloride [C_2C_1im][Cl], and trihexyl(tetradecyl)phosphonium chloride [$P_{6,6,6,14}$][Cl] to specifically evaluate the effect of (1) non-fluorine halogen-based anions, (2) variations in the alkyl chain length, and (3) the cation type.

2. MATERIALS AND METHODS

2.1. Materials. Difluoromethane (HFC-32, CH_2F_2, CAS no. 75-10-5) and pentafluoroethane (HFC-125, CHF_2CF_3, CAS no. 354-33-6) were obtained from The Chemours Company (Newark, DE) with

https://doi.org/10.1021/acssuschemeng.1c06252
ACS Sustainable Chem. Eng. 2022, 10, 816−830

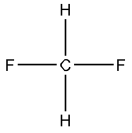

Difluoromethane

HFC-32

Molecular Weight: 52.02 | NBPT = 221.5 K

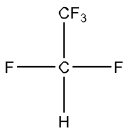

Pentafluoroethane

HFC-125

Molecular Weight: 120.02 | NBPT = 225.06 K

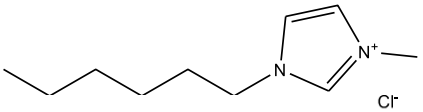

1-*n*-hexyl-3-methylimidazolium chloride

$[C_6C_1im][Cl]$

Molecular Weight: 202.73 | Melting Point: <RT

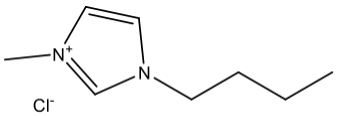

1-*n*-Butyl-3-methylimidazolium chloride

$[C_4C_1im][Cl]$

Molecular Weight: 174.67 | Melting Point: 338.15 to 343.15 K

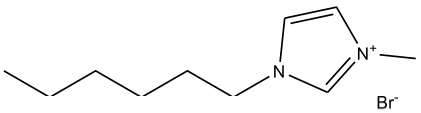

1-*n*-hexyl-3-methylimidazolium bromide

$[C_6C_1im][Br]$

Molecular Weight: 247.18 | Melting Point: <RT

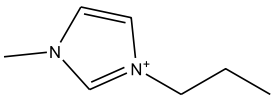

1-Methyl-3-propylimidazolium chloride

$[C_3C_1im][Cl]$

Molecular Weight: 160.65 | Melting Point: 333.15 K

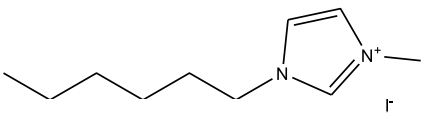

1-*n*-hexyl-3-methylimidazolium iodide

$[C_6C_1im][I]$

Molecular Weight: 294.18 | Melting Point: <RT

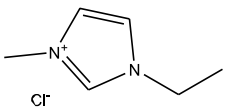

1-Ethyl-3-methylimidazolium chloride

$[C_2C_1im][Cl]$

Molecular Weight: 146.62 | Melting Point: 350.15 to 360.15 K

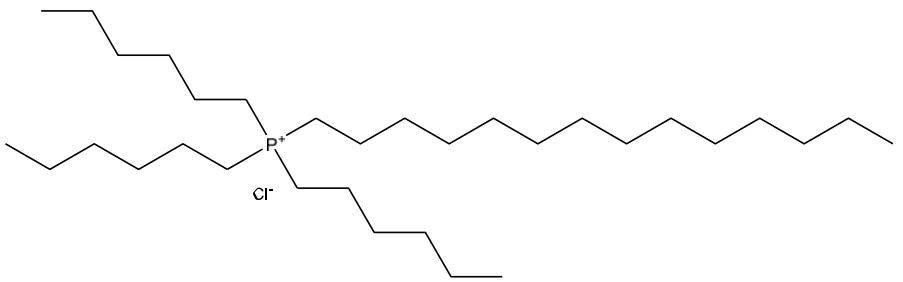

trihexyl(tetradecyl)phosphonium chloride

$[P_{6,6,6,14}][Cl]$

Molecular Weight: 519.32 | Melting Point: <RT

Figure 2. Chemical structures, acronyms, and physical properties of the HFC refrigerants and ILs.[16−18,24,25,27,29,30]

a minimum purity of 99.9 wt % and were used as received. The following ILs were obtained from IoLiTec Ionic Liquid Technologies: 1-*n*-hexyl-3-methylimidazolium iodide ($[C_6C_1im][I]$, assay >98%, CAS no. 178631-05-5, Lot and Filling no. Q00383.1-IL-0026); 1-*n*-hexyl-3-methylimidazolium bromide ($[C_6C_1im][Br]$, assay >99%, CAS no. 85100-78-3, Lot and Filling no. Q00288.7.1-IL-0069); and 1-methyl-3-propylimidazolium chloride ($[C_3C_1im][Cl]$, assay >98%, CAS no. 79917-89-8, Lot and Filling no. Q00183.1.3-IL-0144). 1-*n*-butyl-3-methylimidazolium chloride ($[C_4C_1im][Cl]$, assay ≥98%, CAS no. 79917-90-1, Lot and Filling no. 1185054 23906172) and trihexyl(tetradecyl)phosphonium chloride ($[P_{6,6,6,14}][Cl]$, assay >98%, CAS no. 258864-54-9, Lot and Filling no. 1186190 51505178) were purchased from Fluka Chemika (Switzerland), and 1-ethyl-3-methylimidazolium chloride ($[C_2C_1im][Cl]$, assay >98%, CAS no. 65039-09-0, Lot and Filling no. 1084445 11106247) was purchased from Sigma-Aldrich. HFC-32 and HFC-125 liquid and vapor-phase densities were obtained from the National Institute of Standards and Technology (NIST) REFPROP V.10.0 database.[16] The IL densities, viscosities, and molecular weights were obtained from NIST ILTHERMO V.2.0 database #147 and literature.[17,18] The key chemical properties of the ILs are summarized in Table 1, and the chemical structures, names, and acronyms of the HFCs and ILs are shown in Figure 2.

2.2. Experimental Methodology. The gas absorption measurements were performed using an intelligent gravimetric analyzer (Hiden Isochema Ltd., IGA 003, Warrington, United Kingdom). The experimental equipment and procedures have been described in detail in prior work;[32] therefore, only a summary will be discussed here. For

https://doi.org/10.1021/acssuschemeng.1c06252
ACS Sustainable Chem. Eng. 2022, 10, 816−830

each experiment, approximately 50 mg of IL was added into a flat bottom stainless-steel sample bucket that was loaded into the IGA. The IL sample was degassed under vacuum (10^{-10} MPa) at 348.15 K for a minimum of 12 h or until the mass reading was stable to ensure the removal of any trace amounts of water and/or other volatile impurities from the IL sample. The gas sorption experiments were operated in "static mode", where each pressure set point was maintained by automated adjustments using admit and exhaust valves in the system. Each pressure setpoint was held for a minimum of 8 h to ensure the vapor−liquid equilibrium (VLE) was achieved for the HFC/IL mixture at 298.15 K. The kinetic sorption profile and balance stability were measured using the HISorp software to ensure thermodynamic equilibrium. The temperatures of the sample and counterweight were measured using in situ K-type thermocouples with an uncertainty of ±0.1 K. Pressures under vacuum (10^{-10} to 10^{-5} MPa) were measured using a Pfeiffer vacuum gauge (model PKR251), and pressures from vacuum (10^{-5} MPa) to higher pressure (2.0 MPa) were measured using a Druck pressure transducer (model PDCR4010) with an accuracy of ±0.0008 MPa. Both the pressure transducers and thermocouples were calibrated with NIST-certified reference instruments. The in situ thermocouple for measuring the sample temperature was calibrated using a standard platinum resistance thermometer (Hart Scientific SPRT model 5699/2560 with Hart Scientific Blackstack readout model 1560) with an accuracy of ±0.005 K. The Druck pressure transducer (range 0−2 MPa) was calibrated against a NIST Traceable Paroscientific model 765-1K pressure sensor (range 0−6.89 MPa, serial no. 101314). This instrument is a NIST-certified secondary pressure standard with a traceable accuracy of ±0.0008 MPa. The instrumental uncertainty in T is within ±0.1 K and P is within ±0.001 MPa.

2.3. Equation of State Modeling. In prior work, both cubic equations of state and activity coefficient models have been utilized as analytic methods of representing solubility data, which is necessary for process modeling and optimization frameworks.[15,33−44] In this work, the Peng−Robinson (PR) equation of state (EOS) was used to model the solubility of HFCs in the ILs that were liquid at room temperature (i.e., $[C_6C_1im][I]$, $[C_6C_1im][Br]$, $[C_6C_1im][Cl]$, and $[P_{6,6,6,14}][Cl]$). The PR EOS model is described in detail with eqs 1−15.[45] Two binary interaction parameters were regressed for each HFC/IL mixture, and plots of these fitted models are shown in Figures 3 and 4. The binary interaction parameters are provided in Table 2. The IDAES modeling library was used to perform non-linear least squares regression of the binary interaction parameters with the model described in eqs 1−15.[45] In addition, uncertainty estimates (covariance matrices) for the fitted parameters for each HFC/IL mixture are given in Table S2 in the Supporting Information.

The general form of a cubic EOS is[46]

$$0 = Z^3 - (1 + B - uB)Z^2 + (A - uB - (u - w)B^2)Z - AB - wB^2 - 2B^3 \quad (1)$$

where Z is the compressibility factor of the mixture, and u and w are parameters dependent on the functional form of the EOS, and

$$A = \frac{a_m P}{R^2 T^2} \quad (2)$$

$$B = \frac{b_m P}{RT} \quad (3)$$

Here, a_m and b_m are mixture properties calculated via

$$a_j = \frac{\Omega_A R^2 T_{C,j}^2}{P_{Cj}} \kappa_j \quad (4)$$

$$b_j = \frac{\Omega_B R T_{C,j}}{P_{Cj}} \quad (5)$$

$$a_m = \sum_i \sum_j y_i y_j (a_i a_j)^{1/2} (1 - k_{ij}) \quad (6)$$

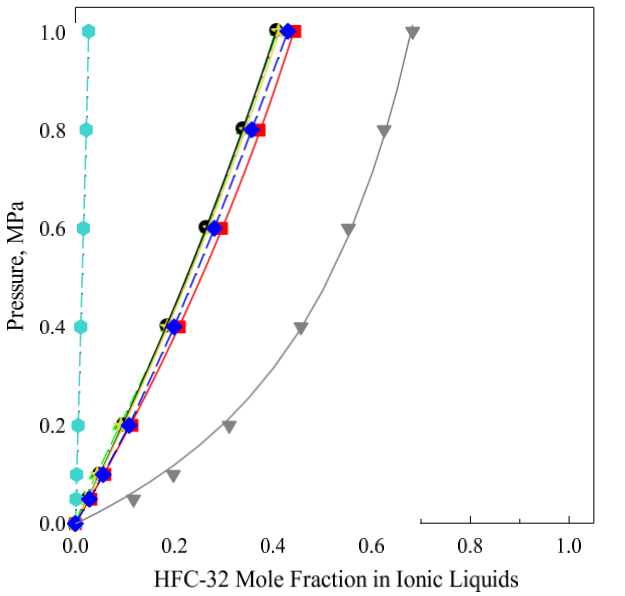

Figure 3. VLE for HFC-32 in $[C_6C_1im][I]$ (black ●), $[C_6C_1im][Br]$ (red ■), $[C_6C_1im][Cl]$ (yellow ★), $[C_4C_1im][Cl]$ (blue ◆), $[C_3C_1im][Cl]$ (green ▲), $[C_2C_1im][Cl]$ (blue ⬢), and $[P_{6,6,6,14}][Cl]$ (gray ▼) at 298.15 K. Symbols are the measured experimental data (PTx), solid lines are the PR EOS model, and dashed lines are guides for the reader. Data for $[C_6C_1im][Cl]$ reported by Morais et al.[15]

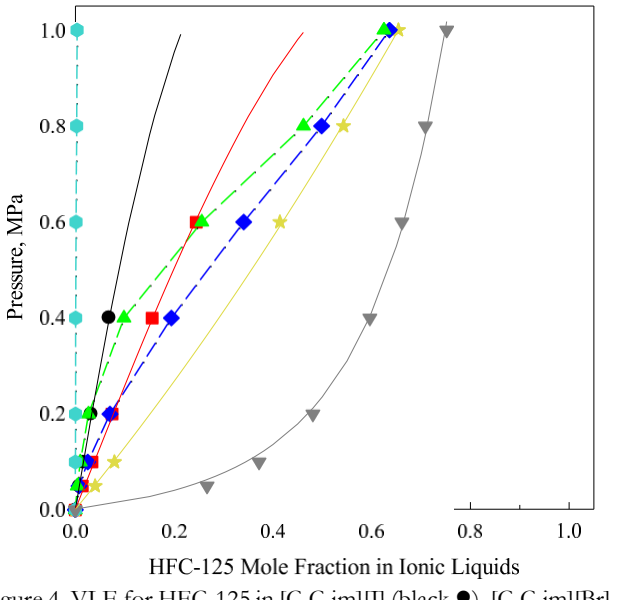

Figure 4. VLE for HFC-125 in $[C_6C_1im][I]$ (black ●), $[C_6C_1im][Br]$ (red ■), $[C_6C_1im][Cl]$ (yellow ★), $[C_4C_1im][Cl]$ (blue ◆), $[C_3C_1im][Cl]$ (green ▲), $[C_2C_1im][Cl]$ (blue ⬢), and $[P_{6,6,6,14}][Cl]$ (gray ▼) at 298.15 K. Symbols are the measured experimental data (PTx), solid lines are the Peng−Robinson EOS model, and dashed lines are guides for the reader. Data for $[C_6C_1im][Cl]$ reported by Morais et al.[15]

$$b_m = \sum_i y_i b_i \quad (7)$$

where P_{Cj} and T_{Cj} are the critical temperature and pressure and y_j is the mole fraction of each component, j. k_{ij} is the set of binary interaction parameters ($k_{ii} = 0$) and Ω_A, Ω_B, and κ_j are parameters specific to a functional form of an EOS.

For the PR EOS

https://doi.org/10.1021/acssuschemeng.1c06252
ACS Sustainable Chem. Eng. 2022, 10, 816−830

Table 2. Binary Interaction Parameters for the PR EOS Model

	HFC-32		HFC-125	
IL	$k_{IL,HFC}$	$k_{HFC,IL}$	$k_{IL,HFC}$	$k_{HFC,IL}$
$[C_6C_1im][I]$	-3.00×10^{-1}	2.94×10^{-2}	9.30×10^{-1}	1.06×10^{-1}
$[C_6C_1im][Br]$	-3.84×10^{-1}	1.03×10^{-2}	1.96×10^{-1}	2.33×10^{-2}
$[C_6C_1im][Cl]$	-2.98×10^{-1}	2.71×10^{-2}	-5.51×10^{-2}	-4.70×10^{-2}
$[P_{6,6,6,14}][Cl]$	-6.47×10^{-1}	-1.35×10^{-1}	-6.89×10^{-1}	-2.65×10^{-1}

$$u = 2 \tag{8}$$

$$w = -1 \tag{9}$$

$$\Omega_A = 0.45724 \tag{10}$$

$$\Omega_B = 0.07780 \tag{11}$$

$$\kappa_j = (1 + (1 - T_{rj}^{2})(0.37464 + 1.54226\omega_j - 0.26992\omega_j^{2}))^2 \tag{12}$$

$$T_r = \frac{T}{T_C} \tag{13}$$

As discussed in previous cubic EOS modeling of HFC/IL systems, the critical temperatures and pressures of ILs must be estimated as pseudocritical points.[47−49] In 2020, Morais et al. specified the critical temperature as 1000 K and critical pressure as 2.5 MPa for all ILs studied;[15] here, we follow this same convention and additionally set the acentric factor (ω_j) to 0.5 for each IL.

The PR EOS written in terms of pressure is

$$P = \frac{RT}{V - b} - \frac{a\alpha}{V^2 + 2bV - b^2} \tag{14}$$

where a and b correspond to a_j and b_j and α corresponds to κ_j.

To fit the parameters k_{ij}, the following least squared optimization formulation was used

$$\min(P_{model} - P_{exp})^2 \tag{15}$$

constrained by eqs 1−15 to calculate P_{model}. P_{exp} are the experimentally measured pressures at equilibrium.

2.4. Henry's Law Constant at Infinite Dilution. Henry's law is the "proportionality, at equilibrium, between the abundance of a species in the gas phase and its abundance in a liquid solution".[50] Experimental Henry's law constants (k_H) were calculated at infinite dilute concentration to evaluate the absorption of the refrigerant in the ILs, where higher refrigerant solubility is indicated by lower k_H values and lower refrigerant solubility is indicated by higher k_H. The solubilities of both HFC-32 and HFC-125 in the HFC/IL systems show a linear increase with increasing pressure up to 0.2 MPa. This allows for the assumption that under dilute conditions, the HFC partial pressure was directly proportional to the HFC composition in the liquid phase. Experimental Henry's law constants can be calculated from experimental HFC solubility (PTx) data assuming the Krichevsky−Kasarnovsky equation is not required for hydrostatic pressure correction[15]

$$k_H = \lim_{x_1 \to 0} \frac{f_1^{V}(T, P, y_1)}{x_1} \approx \left(\frac{df_1^{V}}{dx_1}\right)_{x_1=0} \tag{16}$$

where f_1^{V} is the vapor phase fugacity of HFC ($y_1 = 1$) absorbed in the IL, and x_1 is the mole fraction of HFC absorbed in the IL. The vapor phase fugacities of the HFCs used in this study were obtained from the NIST REFPROP V.10.0 database. The Henry's law constants were calculated by fitting the experimental solubility data (including the theoretical point of zero HFC in the IL at zero pressure) up to 0.2 MPa and determining the slope of a linear regression.

2.5. Fickian Diffusion Analysis. The IGA was also used to measure the time-dependent absorption data for HFC-32 and HFC-125 in the ILs. Kinetic data was measured at 298.15 K for each HFC/IL system at the following pressures: 0.05, 0.1, 0.2, 0.4, 0.6, 0.8, and 1.0 MPa. A detailed description of the application of Fick's law to the experimental data collected in the IGA was previously reported;[35] therefore, only key conditions and assumptions will be discussed here. To apply the simplified Fickian diffusion model, the following assumptions were made: (1) there is only physical interaction between the IL and HFC; (2) a vertical, one-dimensional diffusion process describes the sorption of HFC; (3) there is no convective flow in the IL; (4) at a given T and P a thin boundary layer exists between the IL and HFC, where thermodynamic equilibrium is reached at the saturation concentration (C_S); and (5) the IL/HFC mixture is a highly dilute solution, thus at a given T and P the thermophysical properties are constant. The assumptions describe a local concentration difference that allows for the dissolution of the HFC in ILs to be described using the equation for one-dimensional mass diffusion in the z direction

$$\frac{\partial C}{\partial t} = D\frac{\partial^2 C}{\partial z^2} \tag{17}$$

with the initial condition

$$C = C_0 \text{ at } \quad t = 0 \text{ and } 0 < z < L \tag{18}$$

with the boundary conditions

$$C = C_S \text{ at } \quad t > 0 \text{ and } z = 0 \tag{19}$$

$$\frac{\partial C}{\partial z} = 0 \text{ at } \quad t > 0 \text{ and } z = L \tag{20}$$

where time is t, the concentration of the HFC in the IL as a function of time is C, the vertical location is z (the vapor−liquid boundary is at $z = 0$), the depth of the IL in the sample bucket is L, and the diffusion coefficient is D (assumed to be constant). The depth (L) was estimated by assuming: (1) an even, thin layer of IL was coating the bottom of the sample bucket, (2) the cylindrical geometry of the sample bucket, (3) the sample mass, and (4) the average weight fraction density at a given T and P of the HFC/IL mixture at both the saturated (C_S) and saturation initial (C_0) concentrations. The initial and boundary conditions (eqs 18−20) were used to solve eq 17 analytically using the Laplace transform or separation of variables method

$$C = C_S\left(1 - 2\left(1 - \frac{C_0}{C_S}\right)\sum_{n=0}^{\infty} \frac{\exp(-\lambda_n^2 Dt)\sin \lambda_n z}{L\lambda_n}\right) \tag{21}$$

$$\text{where } \lambda_n = \left(n + \frac{1}{2}\right)\frac{\pi}{L} \tag{22}$$

Equation 21 represents the concentration profile in the z direction, but to fit the experimental data from the IGA it is necessary to have an equation that can model the total concentration of the absorbed gas in the IL. To do this, the equation for space-averaged concentration at a given time ($\langle C \rangle$) is used

$$\langle C \rangle = \int_0^L \frac{C}{L} dz \tag{23}$$

Using eqs 21 and 23, the following equation for $\langle C \rangle$ is obtained

https://doi.org/10.1021/acssuschemeng.1c06252
ACS Sustainable Chem. Eng. 2022, 10, 816−830

$$\langle C \rangle = C_s\left(1 - 2\sum_{n=0}^{\infty} \frac{\exp(-\lambda_n^2 D t)}{L\,\lambda_n}\right) \quad (24)$$

where $\lambda = \left(n + \frac{1}{2}\right)\frac{\pi}{L}$ (25)

Equation 24 was used to calculate the solubility limit at equilibrium (C_s) and the diffusion coefficient (D) for each HFC/IL system using non-linear regression that was performed in MATLAB with the proper selection of the C_0 value to obtain the best model fit. Finally, only the first 10 terms of the infinite summation in eq 24 were necessary.

3. RESULTS AND DISCUSSION

3.1. VLE Results. Isothermal VLE data was gathered at 298.15 K and pressures ranging from 0.05 to 1.0 MPa. Figures 3 and 4 show the equilibrium data for each IL and PR EOS model predictions for [C_6C_1im][I], [C_6C_1im][Br], [C_6C_1im][Cl], and [$P_{6,6,6,14}$][Cl] with HFC-32 and HFC-125, respectively. The [C_4C_1im][Cl], [C_3C_1im][Cl], and [C_2C_1im][Cl] are solid at room temperature and as such were not modeled using the Peng−Robinson EOS. However, it is important to note that for the solubility measurements with [C_4C_1im][Cl] and [C_3C_1im][Cl], both was heated above their melting point during the sample preparation and were in a metastable state for the solubility measurements.[51−53]

The solubility of HFC-32 in the ILs is compared with [C_6C_1im][Cl] from Morais et al. in Figure 3.[15] The solubility for HFC-32 was similar in all the imidazolium-based ILs except for [C_2C_1im][Cl] that had nearly zero solubility. The low sorption of HFC-32 in [C_2C_1im][Cl] is most likely due to the fact that the IL remained a solid during the sorption measurements. The solubility of HFC-32 was higher in [$P_{6,6,6,14}$][Cl] compared with the other imidazolium-based ILs. The high sorption of HFC-32 in [$P_{6,6,6,14}$][Cl] shows how changing the cation from an imidazolium to a phosphonium can significantly affect the refrigerant solubility. A hypothesis for these trends will be discussed further in the next section.

The solubility of HFC-125 in the ILs is compared with [C_6C_1im][Cl] from Morais et al. in Figure 4.[15] The solubility of HFC-125 varies significantly with each IL and the trends will be discussed in the next section. The experimental VLE data for each HFC/IL mixture at 298.15 K and pressures: 0.05, 0.1, 0.2, 0.4, 0.6, 0.8, and 1.0 MPa are provided in Tables 3−9. The maximum pressure of 1.0 MPa was selected to not exceed the saturation vapor pressure of HFC-32 (1.69 MPa) and HFC-125 (1.38 MPa) at 298.15 K.

Prior to measuring the results reported in Tables 3−9, the solubility of HFC-125 was measured in [C_4C_1im][PF_6] to validate the experimental method and T and P calibrations. The results are provided in Figure S1 in the Supporting Information and confirm that the method reproduced prior results within the experimental T, P, and mass uncertainties.

For each IL, the solubility of HFC-32 and HFC-125 increased with increasing pressure, as expected. When comparing the solubility data for designing a separation process, the most important criterion is the relative difference in solubility on a mass fraction basis between HFC-32 and HFC-125 at the same T and P for a given IL. The largest relative difference in solubility on a mass fraction basis between HFC-32 and HFC-125 shown in Tables 2−8 was found with [C_6C_1im][Cl] and [$P_{6,6,6,14}$][Cl]. The solubility of HFC-125 in [C_6C_1im][Cl] was 52.8 wt %, and the solubility of HFC-32 was 15.2 wt % at 298.15 K and 1.0 MPa. The HFC-125 was about 3.5 times more soluble in [C_6C_1im][Cl] compared with HFC-32 at 298.15 K and 1.0 MPa. The solubility of HFC-125 in [$P_{6,6,6,14}$][Cl] was 41.2 wt %, and the solubility of HFC-32 was 17.6 wt % at 298.15 K and 1.0 MPa. The HFC-125 was about 2.3 times more soluble in [$P_{6,6,6,14}$][Cl] compared with HFC-32. The large differences in the HFC-125 and HFC-32

Table 3. Experimental VLE for HFC-32/[C_6C_1im][I] and HFC-125/[C_6C_1im][I] Mixtures at 298.15 K[a]

HFC-32 (1) + [C_6C_1im][I] (2)			HFC-125 (1) + [C_6C_1im][I] (2)		
P (MPa)	$100x_1$ (mol %)	w_1 (wt %)	P (MPa)	$100x_1$ (mol %)	w_1 (wt %)
0.00	0.0	0.0	0.00	0.0	0.0
0.05	2.5	0.5	0.05	0.8	0.3
0.1	4.8	0.9	0.1	1.6	0.7
0.2	9.7	1.9	0.2	3.1	1.3
0.4	18.5	3.9	0.4	6.8	2.9
0.6	26.4	6.0	0.6	10.8	4.7
0.8	33.8	8.3	0.8	16.1	7.2
1.0	40.6	10.8	1.0	21.3	10.0

[a]P = pressure; $100x_1$ and w_1 = HFC composition (mol % and wt %) in the IL. Standard uncertainties: $u(T)$ = 0.1 K, $u(P)$ = 0.0008 MPa, and $u(100x_1)$ = 0.5 mol %.

Table 4. Experimental VLE for HFC-32/[C_6C_1im][Br] and HFC-125/[C_6C_1im][Br] Mixtures at 298.15 K[a]

HFC-32 (1) + [C_6C_1im][Br] (2)			HFC-125 (1) + [C_6C_1im][Br] (2)		
P (MPa)	$100x_1$ (mol %)	w_1 (wt %)	P (MPa)	$100x_1$ (mol %)	w_1 (wt %)
0.00	0.0	0.0	0.00	0.0	0.0
0.05	3.1	0.7	0.05	1.4	0.7
0.1	6.0	1.3	0.1	3.3	1.7
0.2	11.4	2.6	0.2	7.4	3.7
0.4	21.0	5.3	0.4	15.5	8.2
0.6	29.5	8.1	0.6	24.5	13.6
0.8	37.1	11.0	0.8	34.3	20.2
1.0	44.3	14.3	1.0	46.2	29.4

[a]P = pressure; $100x_1$ and w_1 = HFC composition (mol % and wt %) in the IL. Standard uncertainties: $u(T)$ = 0.1 K, $u(P)$ = 0.0008 MPa, and $u(100x_1)$ = 0.5 mol %.

Table 5. Experimental VLE for HFC-32/[C_6C_1im][Cl] and HFC-125/[C_6C_1im][Cl] Mixtures at 298.15 K Reported by Morais et al[15]

HFC-32 (1) + [C_6C_1im][Cl] (2)[a]			HFC-125 (1) + [C_6C_1im][Cl] (2)[a]		
P (MPa)	$100x_1$ (mol %)	w_1 (wt %)	P (MPa)	$100x_1$ (mol %)	w_1 (wt %)
0.00	0.0	0.0	0.00	0.0	0.0
0.05	2.1	0.5	0.05	4.0	2.4
0.1	4.4	1.2	0.1	7.9	4.8
0.2	9.2	2.5	0.2	16.0	10.2
0.4	18.6	5.6	0.4	29.0	19.5
0.6	27.2	8.8	0.6	41.4	29.6
0.8	34.5	11.9	0.8	54.3	41.3
1.0	41.0	15.2	1.0	65.4	52.8

[a]P = pressure; $100x_1$ and w_1 = HFC composition (mol % and wt %) in the IL. Standard uncertainties: $u(T)$ = 0.1 K, $u(P)$ = 0.0008 MPa, and $u(100x_1)$ = 0.5 mol %.

https://doi.org/10.1021/acssuschemeng.1c06252
ACS Sustainable Chem. Eng. 2022, 10, 816−830

Table 6. Experimental VLE for HFC-32/[C_4C_1im][Cl] and HFC-125/[C_4C_1im][Cl] Mixtures at 298.15 K[a]

HFC-32 (1) + [C_4C_1im][Cl] (2)			HFC-125 (1) + [C_4C_1im][Cl] (2)		
P (MPa)	$100x_1$ (mol %)	w_1 (wt %)	P (MPa)	$100x_1$ (mol %)	w_1 (wt %)
0.00	0.0	0.0	0.00	0.0	0.0
0.05	2.8	0.9	0.05	0.8	0.5
0.1	5.6	1.7	0.1	2.5	1.7
0.2	10.9	3.5	0.2	7.0	4.9
0.4	20.0	6.9	0.4	19.4	14.2
0.6	28.1	10.4	0.6	34.1	26.2
0.8	35.6	14.1	0.8	49.9	40.6
1.0	42.9	18.3	1.0	63.6	54.5

[a]P□pressure; $100x_1$ and w_1□HFC composition (mol % and wt %) in the IL. Standard uncertainties: $u(T)$ = 0.1 K, $u(P)$ = 0.0008 MPa, and $u(100x_1)$ = 0.5 mol %.

Table 7. Experimental VLE for HFC-32/[C_3C_1im][Cl] and HFC-125/[C_3C_1im][Cl] Mixtures at 298.15 K[a]

HFC-32 (1) + [C_3C_1im][Cl] (2)			HFC-125 (1) + [C_3C_1im][Cl] (2)		
P (MPa)	$100x_1$ (mol %)	w_1 (wt %)	P (MPa)	$100x_1$ (mol %)	w_1 (wt %)
0.00	0.0	0.0	0.00	0.0	0.0
0.05	1.9	0.6	0.05	0.4	0.3
0.1	4.3	1.4	0.1	1.0	0.8
0.2	9.0	3.1	0.2	2.7	2.0
0.4	18.6	6.9	0.4	9.8	7.5
0.6	26.6	10.5	0.6	25.6	20.4
0.8	33.9	14.2	0.8	46.2	39.0
1.0	40.7	18.2	1.0	62.5	55.4

[a]P□pressure; $100x_1$ and w_1□HFC composition (mol % and wt %) in the IL. Standard uncertainties: $u(T)$ = 0.1 K, $u(P)$ = 0.0008 MPa, and $u(100x_1)$ = 0.5 mol %.

Table 8. Experimental VLE for HFC-32/[C_2C_1im][Cl] and HFC-125/[C_2C_1im][Cl] Mixtures at 298.15 K[a]

HFC-32 (1) + [C_2C_1im][Cl] (2)			HFC-125 (1) + [C_2C_1im][Cl] (2)		
P (MPa)	$100x_1$ (mol %)	w_1 (wt %)	P (MPa)	$100x_1$ (mol %)	w_1 (wt %)
0.00	0.0	0.0	0.00	0.0	0.0
0.05	0.1	0.1	0.05	0.0	0.0
0.1	0.3	0.1	0.1	0.0	0.0
0.2	0.6	0.2	0.2	0.0	0.0
0.4	1.1	0.4	0.4	0.1	0.1
0.6	1.6	0.6	0.6	0.1	0.1
0.8	2.2	0.8	0.8	0.3	0.2
1.0	2.7	1.0	1.0	0.3	0.3

[a]P□pressure; $100x_1$ and w_1□HFC composition (mol % and wt %) in the IL. Standard uncertainties: $u(T)$ = 0.1 K, $u(P)$ = 0.0008 MPa, and $u(100x_1)$ = 0.5 mol %.

solubilities make both [C_6C_1im][Cl] and [$P_{6,6,6,14}$][Cl] potential entrainers for the separation of R-410A using extractive distillation.

3.2. Anion Comparison. The solubilities of HFC-32 and HFC-125 in [C_6C_1im][I] and [C_6C_1im][Br] were compared to the data for [C_6C_1im][Cl] from Morais et al. in Figure 5 to understand the effects of varying the halogen anion.[15] In Figure 5, plots (A,C,E) show the relative difference in solubility on a mole fraction basis between HFC-32 and HFC-125 with each IL. The solubility of HFC-32 in terms of mole fraction remains relatively constant between the three anions; however, there is a distinct difference in the solubility of HFC-125 as the anion is varied as shown in Figure 5 and Table 10.

Table 9. Experimental VLE for HFC-32/[$P_{6,6,6,14}$][Cl] and HFC-125/[$P_{6,6,6,14}$][Cl] Mixtures at 298.15 K[a]

HFC-32 (1) + [$P_{6,6,6,14}$][[Cl] (2)			HFC-125 (1) + [$P_{6,6,6,14}$][[Cl] (2)		
P (MPa)	$100x_1$ (mol %)	w_1 (wt %)	P (MPa)	$100x_1$ (mol %)	w_1 (wt %)
0.00	0.0	0.0	0.00	0.0	0.0
0.05	11.8	1.3	0.05	26.7	7.8
0.1	19.8	2.4	0.1	37.2	12.0
0.2	31.1	4.3	0.2	48.1	17.6
0.4	45.6	7.7	0.4	59.6	25.4
0.6	55.2	11.0	0.6	66.1	31.1
0.8	62.3	14.2	0.8	70.9	36.0
1.0	68.1	17.6	1.0	75.2	41.2

[a]P□pressure; $100x_1$ and w_1□HFC composition (mol % and wt %) in the IL. Standard uncertainties: $u(T)$ = 0.1 K, $u(P)$ = 0.0008 MPa, and $u(100x_1)$ = 0.5 mol %.

HFC-125 has lower solubility than HFC-32 in [C_6C_1im][I], has similar solubility to HFC-32 in [C_6C_1im][Br], and has higher solubility than HFC-32 in [C_6C_1im][Cl]. Although it is clear the variation of the anion influences the solubility of HFC-125, there are no clear solubility trends until the differences in molecular weight are considered ($MW_{HFC\text{-}32}$ = 52.024 g·mol^{-1} and $MW_{HFC\text{-}125}$ = 120.02 g·mol^{-1}), as shown in Figure 5 plots (B,D,F). The HFC-32 solubility again shows little difference between the anions, but the HFC-125 shows a clear trend: as the size of the anion decreases, strength of Lewis basicity increases, and the electronegativity of the anion increases, the solubility of HFC-125 increases as shown in Figure 5 and Table 11.

The relative difference in solubility on a mass fraction basis between HFC-32 and HFC-125 is almost negligible in [C_6C_1im][I] and still relatively small in [C_6C_1im][Br], meaning neither would be good candidates as entrainers in extractive distillation for the separation of R-410A.

3.3. Alkyl Chain Length Comparison. The solubility for HFC-32 and HFC-125 in [C_4C_1im][Cl], [C_3C_1im][Cl], and [C_2C_1im][Cl] is compared to [C_6C_1im][Cl] from Morais et al. in Figure 6 to compare the effects of varying the alkyl chain length.[15] Note that [C_4C_1im][Cl], [C_3C_1im][Cl], and [C_2C_1im][Cl] are all solids at room temperature, while [C_6C_1im][Cl] is a liquid. In addition, [C_2C_1im][Cl] is assumed to have remained a solid throughout the solubility experiments, while [C_4C_1im][Cl] and [C_3C_1im][Cl] are in a metastable liquid state. High-pressure view cell experiments were conducted under the same T and P conditions as the IGA to confirm the solid−liquid phase transitions, see Figure S2 in the Supporting Information for details.

In Figure 6, plots (A,C,E,G) show the relative difference in solubility on a mole fraction basis between HFC-32 and HFC-125 with each IL. The solubility of HFC-32 in terms of mole fraction remains relatively constant among [C_6C_1im][Cl], [C_4C_1im][Cl], and [C_3C_1im][Cl], suggesting that the solubility of HFC-32 in the metastable state for [C_4C_1im][Cl] and [C_3C_1im][Cl] behave the same as [C_6C_1im][Cl] in the liquid state. However, HFC-32 solubility in [C_2C_1im][Cl] is

https://doi.org/10.1021/acssuschemeng.1c06252
ACS Sustainable Chem. Eng. 2022, 10, 816−830

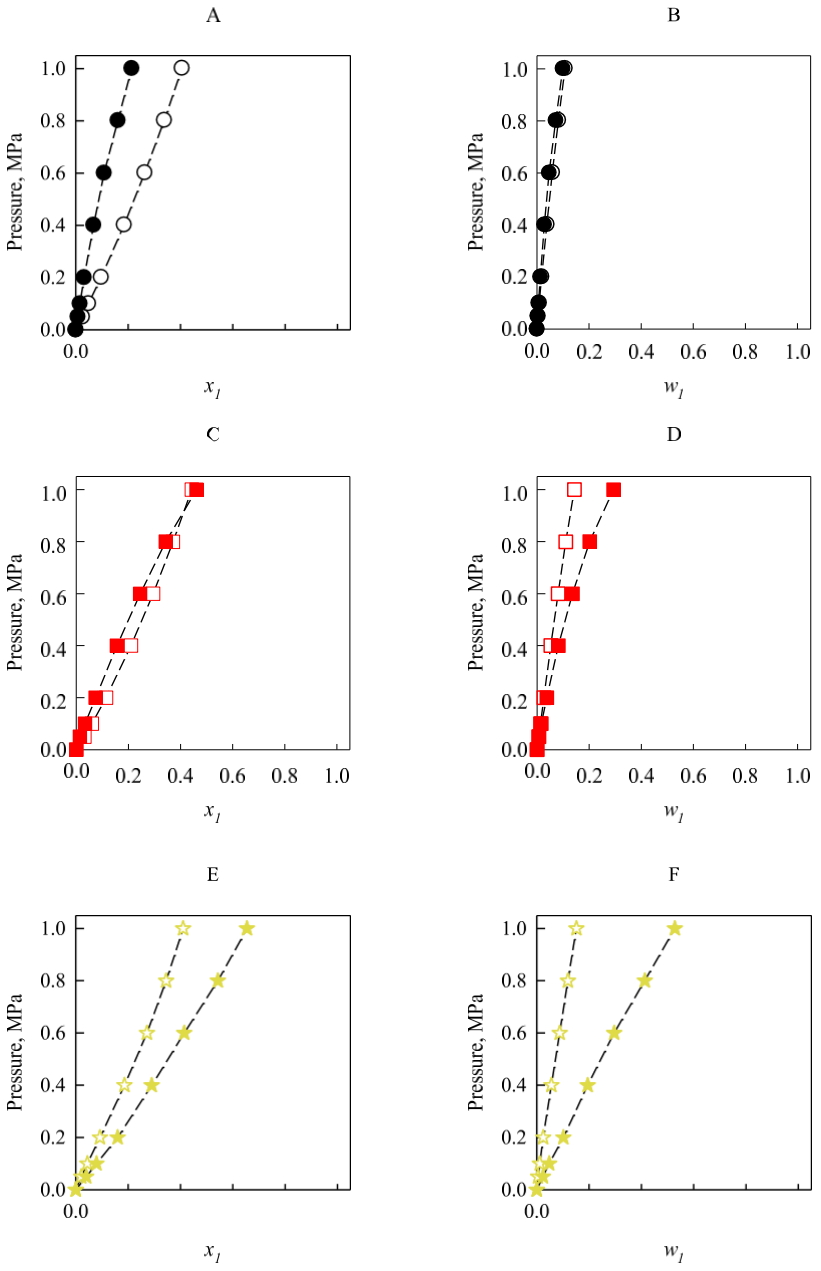

Figure 5. Effect of anions on VLE (mol fraction, x_1 and mass fraction, w_1) for HFC-32 and HFC-125 in ILs at 298.15 K: (A) HFC x_1 in $[C_6C_1im][I]$ (○, ●), (B) HFC w_1 in$[C_6C_1im][I]$ (○, ●), (C) HFC x_1 in $[C_6C_1im][Br]$ (red □, red ■), (D) HFC w_1 in $[C_6C_1im][Br]$ (red □, red ■), (E) HFC x_1 in $[C_6C_1im][Cl]$ (yellow ☆, yellow ★), and (F) HFC w_1 in $[C_6C_1im][Cl]$ (yellow ☆, yellow ★). Symbols are the measured experimental data (*PTx*) for HFC-32 (open symbols) and HFC-125 (solid symbols). Dashed lines are guides for the reader. Data for $[C_6C_1im][Cl]$ reported by Morais et al.[15]

Table 10. HFC-32 and HFC-125 Solubility ($100x_1$) for $[C_6C_1im][I]$, $[C_6C_1im][Br]$, and $[C_6C_1im][Cl]$ at 298.15 K and 1.0 MPa[a]

	$100x_1$ (mol %) of HFC (1) + IL (2)		
	$[C_6C_1im][I]$	$[C_6C_1im][Br]$	$[C_6C_1im][Cl]$
HFC-32	40.6	44.3	41.0
HFC-125	21.3	46.2	65.4

[a]Data for $[C_6C_1im][Cl]$ reported by Morais et al.[15]

Table 11. HFC-32 and HFC-125 Solubility (w_1) for $[C_6C_1im][I]$, $[C_6C_1im][Br]$, and $[C_6C_1im][Cl]$ at 298.15 K and 1.0 MPa[a]

	w_1 (wt %) of HFC (1) + IL (2)		
	$[C_6C_1im][I]$	$[C_6C_1im][Br]$	$[C_6C_1im][Cl]$
HFC-32	10.8	14.3	15.2
HFC-125	10.0	29.4	52.8

[a]Data for $[C_6C_1im][Cl]$ reported by Morais et al.[15]

distinctly lower than $[C_6C_1im][Cl]$, due to its solid state. The same observations can be made for the solubility of HFC-32 in terms of mass fraction as shown in Figure 6, plots (B,D,F,H).

The solubility of HFC-125 in terms of mole fraction behaves as expected showing higher solubility in the liquid $[C_6C_1im][Cl]$ and lower solubility in the solid $[C_2C_1im][Cl]$. The solubility

https://doi.org/10.1021/acssuschemeng.1c06252
ACS Sustainable Chem. Eng. 2022, 10, 816−830

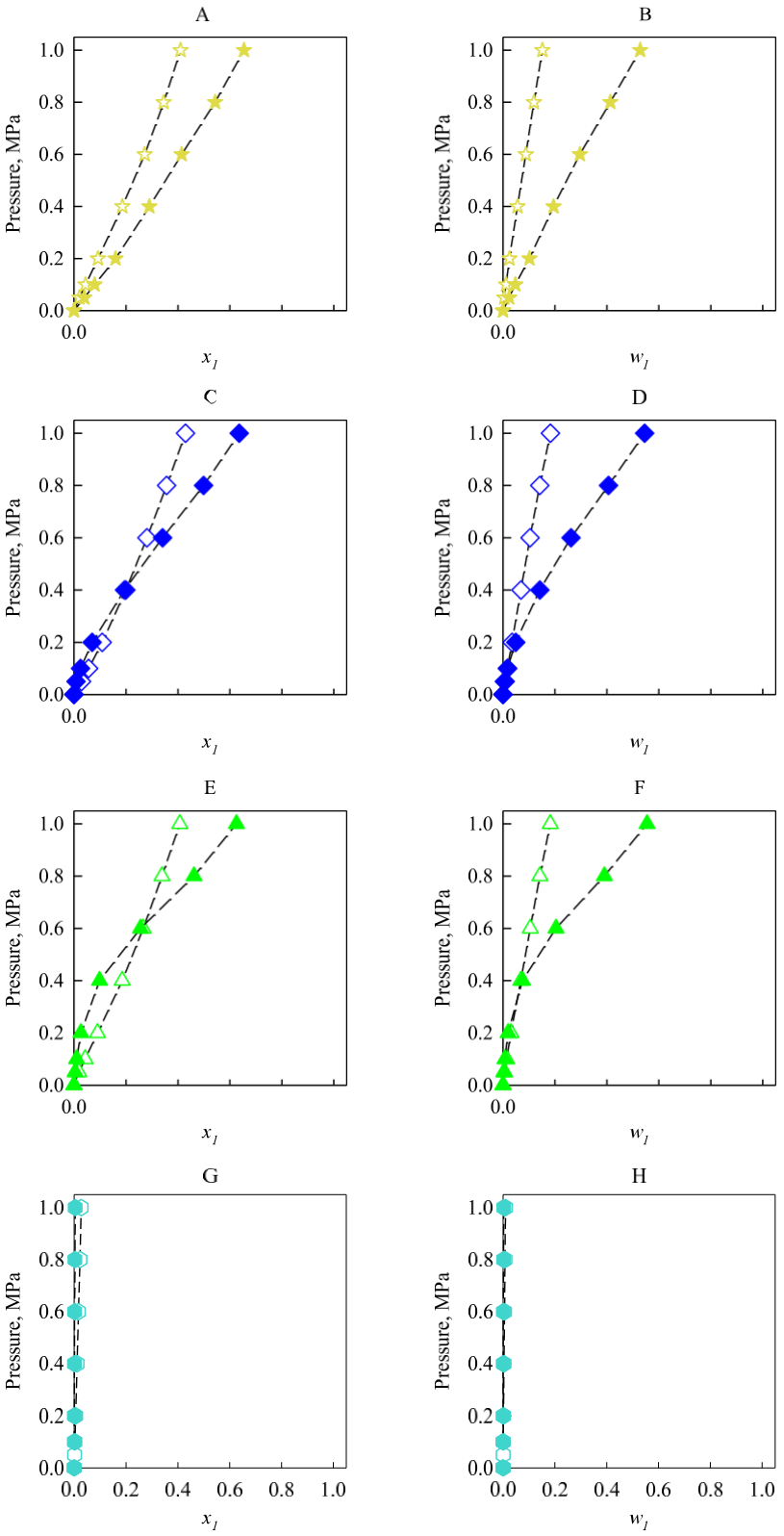

Figure 6. Effects of alkyl chain length on VLE (mol fraction, x_1 and mass fraction, w_1) for HFC-32 and HFC-125 in ILs at 298.15 K: (A) HFC x_1 in $[C_6C_1im][Cl]$ (yellow ☆, yellow ★), (B) HFC w_1 in $[C_6C_1im][Cl]$ (yellow ☆, yellow ★), (C) HFC x_1 in $[C_4C_1im][Cl]$ (blue ◇, blue ◆), (D) HFC w_1 in $[C_4C_1im][Cl]$ (blue ◇, blue ◆), (E) HFC x_1 in $[C_3C_1im][Cl]$ (green ▵, green ▲), (F) HFC w_1 in $[C_3C_1im][Cl]$ (green ▵, green ▲), (G) HFC x_1 in $[C_2C_1im][Cl]$ (blue ⬡, blue ⬢), and (H) HFC w_1 in $[C_2C_1im][Cl]$ (blue ⬡, blue ⬢). Symbols are the measured experimental data (PTx) for HFC-32 (open symbols) and HFC-125 (solid symbols). Dashed lines are guides for the reader. Data for $[C_6C_1im][Cl]$ reported by Morais et al.[15]

https://doi.org/10.1021/acssuschemeng.1c06252
ACS Sustainable Chem. Eng. 2022, 10, 816−830

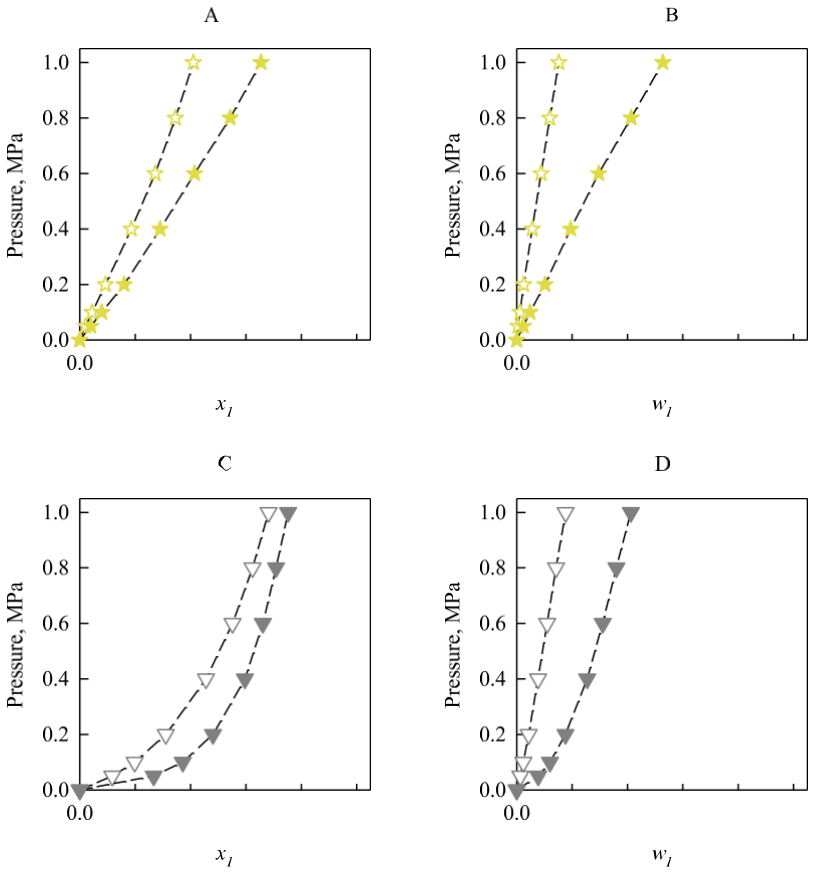

Figure 7. Effects of cations on VLE (mol fraction, x_1 and mass fraction, w_1) for HFC-32 and HFC-125 in ILs at 298.15 K: (A) HFC x_1 in $[C_6C_1im][Cl]$ (yellow ☆, yellow ★), (B) HFC w_1 in $[C_6C_1im][Cl]$ (yellow ☆, yellow ★), (C) HFC x_1 in $[P_{6,6,6,14}][Cl]$ (gray ▽, gray ▼), and (D) HFC w_1 in $[P_{6,6,6,14}][Cl]$ (gray ▽, gray ▼). Symbols are the measured experimental data (PTx) for HFC-32 (open symbols) and HFC-125 (solid symbols). Dashed lines are guides for the reader. Data for $[C_6C_1im][Cl]$ reported by Morais et al.[15]

of $[C_4C_1im][Cl]$ and $[C_3C_1im][Cl]$ as a function of P at constant T has an unusual shape due to a distinct change in the slope that leads to the intersection of the HFC-32 and HFC-125 isotherms. We hypothesize this change in the slope occurs due to the increase in HFC-125 solubility as the viscosity changes with gas sorption. View cell experiments support this assumption based on the visual appearance of the IL as the HFC-125 pressure was increased in discrete increments at a constant temperature of 298.15 K. For both $[C_4C_1im][Cl]$ and $[C_3C_1im][Cl]$ at a pressure of about 0.4 MPa, the IL appearance changed from a viscous liquid to a non-viscous liquid as shown in the Supporting Information (see Figure S3). The solubility trends in the mass fraction become clearer when the differences in the molecular weight are considered ($MW_{HFC\text{-}32}$ = 52.024 g·mol^{-1} and $MW_{HFC\text{-}125}$ = 120.02 g·mol^{-1}), as shown in Figure 6, plots (B,D,F,H). HFC-125 shows a general trend: as the alkyl chain length increases, van der Waals forces increase resulting in an increase in HFC-125 solubility. HFC-125 is an electron donor and the alkyl chains are electron acceptors. As the alkyl chain length increases, so does the interaction with HFC-125. One interesting trend seen in $[C_4C_1im][Cl]$ and $[C_3C_1im][Cl]$ is the solubility of HFC-125 is similar to that of HFC-32 at low pressures. As pressure increases and the solubility of HFC-125 increases, the slope changes (as seen in Figure 6D,F) and the solubility of HFC-125 at 1 MPa and 298.15 K in both is very similar to the solubility found in $[C_6C_1im][Cl]$ under the same conditions. For this reason, the relative difference in solubility between HFC-32 and HFC-125 at pressures greater than 0.4 MPa suggests that $[C_4C_1im][Cl]$ and $[C_3C_1im][Cl]$ could also be potential entrainers for the separation of R-410A using extractive distillation.

3.4. Cation Comparison. To compare the effects of different cations, the solubility for HFC-32 and HFC-125 in $[P_{6,6,6,14}][Cl]$ is compared to that in $[C_6C_1im][Cl]$ reported by Morais et al. in Figure 7 and Tables 12 and 13.[15] In Figure 7,

Table 12. HFC-32 and HFC-125 Solubility ($100x_1$) for $[P_{6,6,6,14}][Cl]$ and $[C_6C_1im][Cl]$ at 298.15 K and 1.0 MPa[a]

	$100x1$ (mol %) of HFC (1) + IL (2)	
	$[P_{6,6,6,14}][Cl]$	$[C_6C_1im][Cl]$
HFC-32	68.1	41.0
HFC-125	75.2	65.4

[a]Data for $[C_6C_1im][Cl]$ reported by Morais et al.[15]

Table 13. HFC-32 and HFC-125 Solubility (w_1) for $[P_{6,6,6,14}][Cl]$ and $[C_6C_1im][Cl]$ at 298.15 K and 1.0 MPa[a]

	w_1 (wt %) of HFC (1) + IL (2)	
	$[P_{6,6,6,14}][Cl]$	$[C_6C_1im][Cl]$
HFC-32	17.6	15.2
HFC-125	41.2	52.8

[a]Data for $[C_6C_1im][Cl]$ reported by Morais et al.[15]

https://doi.org/10.1021/acssuschemeng.1c06252
ACS Sustainable Chem. Eng. 2022, 10, 816−830

plots (A,C) show the relative difference in solubility on a mole fraction basis between HFC-32 and HFC-125 in both ILs. The solubility difference of HFC-32 and HFC-125 in terms of the mole fraction and weight fraction remains relatively constant between the two cations; however, there is a distinct difference at low-pressures, where the phosphonium-based cation has much higher HFC solubility compared with the imidazolium-based cation as shown in Figure 7, plots (A,B) versus plots (C,D). This difference may be due to the longer alkyl chains in the phosphonium-based cation interacting through van der Waals forces with the HFC and an increase in the free volume.

3.5. Deviation from Ideality (Raoult's Law). The normalized fugacity of HFC-32 and HFC-125 was plotted against the HFC mole fraction in the IL to evaluate the non-ideality of each system and was compared to $[C_6C_1im][Cl]$ from Morais et al.[15] The normalized fugacity was calculated by dividing the vapor-phase fugacity (f^v) of the HFC by the fugacity of the HFC at saturated vapor pressure (f^{sat}) for 298.15 K. This expression is valid due to the negligible vapor pressure of the IL, where the gas phase is essentially pure HFC ($y_{HFC\text{-}32} = 1$ and $y_{HFC\text{-}125} = 1$).

Figure 8 shows the normalized fugacity of HFC-32 as a function of the mole fraction solubility in the IL with

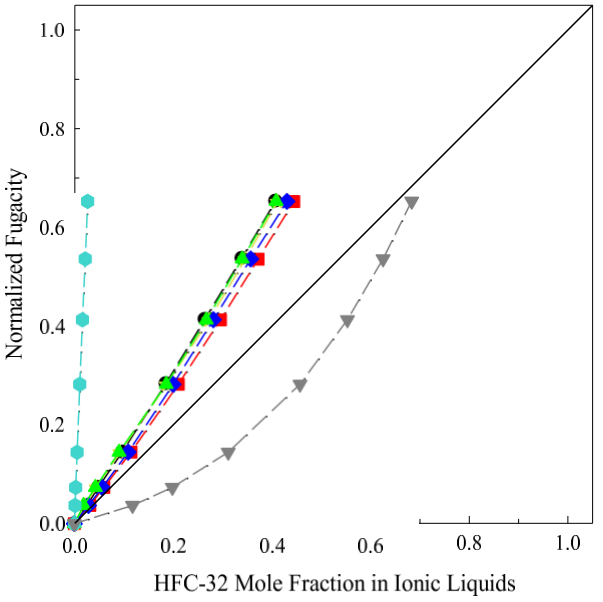

Figure 8. Normalized fugacity for HFC-32 in $[C_6C_1im][I]$ (●), $[C_6C_1im][Br]$ (red ■), $[C_6C_1im][Cl]$ (yellow ★), $[C_4C_1im][Cl]$ (blue ◆), $[C_3C_1im][Cl]$ (green ▲), $[C_2C_1im][Cl]$ (blue ⬢), and $[P_{6,6,6,14}][Cl]$ (gray ▼) as a function of HFC molar composition at 298.15 K. The solid line represents Raoult's law, and the dashed lines are guides for the reader. Data for $[C_6C_1im][Cl]$ reported by Morais et al.[15]

comparison to Raoult's law at 298.15 K. All the imidazolium-based ILs with HFC-32 show similar positive deviations from ideality despite different anions and alkyl chain lengths except for $[C_2C_1im][Cl]$, which shows a much higher positive deviation (i.e., weaker interactions) due to remaining a solid throughout the solubility experiments. The phosphonium-based IL ($[P_{6,6,6,14}][Cl]$) with HFC-32 is the only IL in this study that shows a negative deviation from ideality (i.e., stronger interactions). However, HFC-32 with $[P_{6,6,6,14}][Cl]$ has an interesting shape that shows an ideal behavior at both low and high HFC mole fractions and the largest negative deviations between 0.3 and 0.6 HFC-32 mol fraction suggesting strong interactions of HFC-32 with the IL.

Figure 9 shows the normalized fugacity of HFC-125 as a function of the mole fraction solubility in the IL with

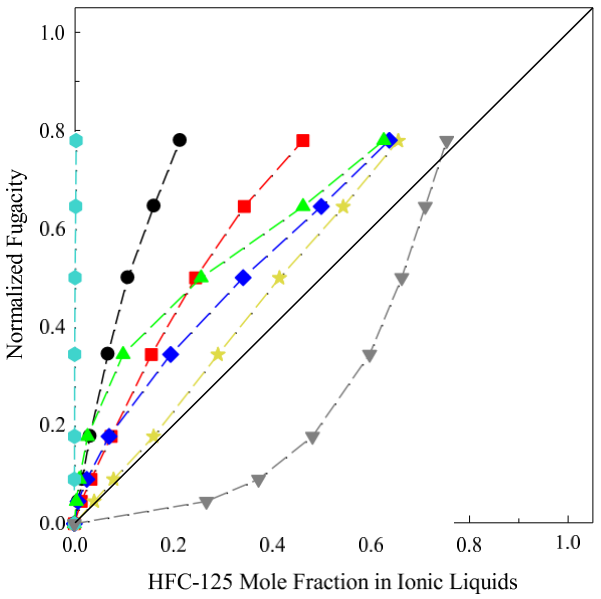

Figure 9. Normalized fugacity for HFC-125 in $[C_6C_1im][I]$ (●), $[C_6C_1im][Br]$ (red ■), $[C_6C_1im][Cl]$ (yellow ★), $[C_4C_1im][Cl]$ (blue ◆), $[C_3C_1im][Cl]$ (green ▲), $[C_2C_1im][Cl]$ (blue ⬢), and $[P_{6,6,6,14}][Cl]$ (gray ▼) as a function of HFC molar composition at 298.15 K. Solid line represents Raoult's law and dashed lines are guides for the reader. Data for $[C_6C_1im][Cl]$ reported by Morais et al.[15]

comparison to Raoult's law at 298.15 K. In comparison with the HFC-32/IL systems, the HFC-125/IL systems have significantly more variation in non-ideality from each other. Again, all the imidazolium-based ILs with HFC-125 display positive deviations from ideality; however, there is clear differences seen between the anion, alkyl chain length, and IL phase. As the size of the anion increases, the strength of Lewis basicity decreases, and the electronegativity of the anion decreases, so the HFC-125/IL systems increase in positive deviation from Raoult's law (i.e., weaker interactions between HFC-125 and the IL). Similarly, as the alkyl chain length decreases ($C_6 > C_4 > C_3 > C_2$), van der Waals forces decrease, so the HFC-125/IL systems increase in positive deviation from Raoult's law (i.e., weaker interactions between HFC-125 and the IL). The phosphonium-based IL ($[P_{6,6,6,14}][Cl]$) with HFC-125 shows both negative and positive deviation from ideality, with positive deviation occurring at the highest concentration of HFC-125 ($x_1 > 0.7$). The same interesting shape found with HFC-32 is also seen in HFC-125 with an even more exaggerated difference at both low and high mole fractions, with the largest negative deviation occurring between about 0.4 to 0.6 mol fraction HFC-125 in $[P_{6,6,6,14}][Cl]$ suggesting strong interactions of HFC-125 with the cation.

3.6. Ideal Selectivity Based on Henry's Law Constants. Ideal selectivity can be used for comparison to evaluate ILs for the separation of HFC-32 and HFC-125. For this study, two definitions of ideal selectivity were selected. The first

https://doi.org/10.1021/acssuschemeng.1c06252
ACS Sustainable Chem. Eng. 2022, 10, 816−830

definition is the ratio of the HFC's Henry's law constants at a given temperature

$$S_{Hij} = \left(\frac{k_{Hi}}{k_{Hj}}\right)_T \quad (26)$$

where k_{Hi} and k_{Hj} (i = HFC-32 and j = HFC-125) are the experimental Henry's law constants for the HFCs and T = 298.15 K, as discussed in Section 2.4. The second definition used is the ratio of pure HFC solubilities on a mass basis

$$S_{Wij} = \left(\frac{w_{vi}/w_{li}}{w_{vj}/w_{lj}}\right)_{T,P} \quad (27)$$

where w_{li} and w_{lj} are the liquid mass fractions for the HFCs in the IL (i = HFC-32 and j = HFC-125) at P = 1 MPa and T = 298.15 K. The vapor mass fractions of the HFCs are assumed to be equal to 1.0 (i.e., w_{vi} = 1.0 and w_{vj} = 1.0) because the IL has such a low vapor pressure (e.g., < 1.0 × 10^{-3} to 1.0 × 10^{-5} Pa).

The experimental Henry's law constants, ideal selectivity based on the ratio of the experimental Henry's law constants, and ideal selectivity based on the ratio of pure HFC solubilities on a mass basis are summarized in Table 14 and compared to those obtained in [C_6C_1im][Cl] from Morais et al.[15] Due to [C_2C_1im][Cl] being a solid, k_H (MPa) values were not calculated. All the k_H (MPa) values for HFC-32 in the imidazolium-based ILs at 298.15 K remain relatively constant, ranging from 1.71 to 2.13 MPa. The comparison of all k_H (MPa) values for HFC-32 show the following order: [$P_{6,6,6,14}$][Cl] < [C_6C_1im][Br] < [C_4C_1im][Cl] < [C_6C_1im]-[Cl] < [C_6C_1im][I] < [C_3C_1im][Cl]. The k_H (MPa) values for HFC-125 and the imidazolium-based ILs at 298.15 K range from 1.16 to 6.96 MPa. The comparison of all k_{Hij} (MPa) values for HFC-125 show the following order: [$P_{6,6,6,14}$][Cl] < [C_6C_1im][Cl] < [C_6C_1im][Br] < [C_4C_1im][Cl] < [C_6C_1im]-[I] < [C_3C_1im][Cl]. The solubility trends shown in Figures 3 and 4 agree with the trends shown here. It is clear that the [$P_{6,6,6,14}$][Cl] IL has the lowest k_{Hij} (MPa) values (i.e., highest solubility) for both HFC-32 and HFC-125 as shown in Table 14.

Table 14. Henry's Law Constants (MPa) for HFC-32 and HFC-125 in ILs at 298.15 K, and Selectivity Based on (1) Henry's Law Constants (S_{Hij}) in the ILs at 298.15 K and (2) the Ratio of the Mass Fractions (S_{Wij}) in the ILs at 1.0 MPa and 298.15 K[a,b]

	Henry's law constants (kH, MPa)		selectivity	selectivity
ionic liquid	HFC-32	HFC-125	S_{Hij}	S_{Wij}
[C_6C_1im][I]	2.03 ± 0.02	6.17 ± 0.05	0.33	0.73
[C_6C_1im][Br]	1.71 ± 0.03	2.56 ± 0.15	0.67	1.26
[C_6C_1im][Cl]	2.00 ± 0.00	1.16 ± 0.03	1.72	4.00
[C_4C_1im][Cl]	1.80 ± 0.02	2.59 ± 0.35	0.69	1.00
[C_3C_1im][Cl]	2.13 ± 0.08	6.96 ± 0.79	0.31	0.53
[C_2C_1im][Cl]				0.13
[$P_{6,6,6,14}$][Cl]	0.63 ± 0.08	0.37 ± 0.11	1.68	4.99

[a]Uncertainties are the standard error of the coefficient obtained in the linear regression. [b]Data for [C_6C_1im][Cl] reported by Morais et al.[15]

The ideal selectivity for both S_{Hij} and S_{Wij} increases as the size of the anion decreases and the strength of Lewis basicity and the electronegativity of the anion increases as shown in Figure 10. As the alkyl chain length decreases, van der Waals forces decrease, resulting in a decrease in the ideal selectivity. The [$P_{6,6,6,14}$][Cl] and [C_6C_1im][Cl] have the highest selectivity (S_{Hij} and S_{Wij}) compared with the other ILs.

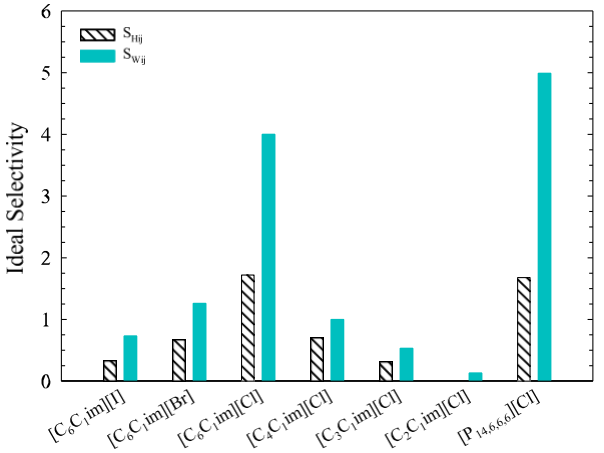

Figure 10. Ideal selectivity for the sorption of HFC-32 and HFC-125 in [C_6C_1im][I], [C_6C_1im][Br], [C_6C_1im][Cl], [C_4C_1im][Cl], [C_3C_1im][Cl], [C_2C_1im][Cl], and [$P_{6,6,6,14}$][Cl]. Open bars with a diagonal pattern represent the ideal selectivity calculated from the ratio of experimental Henry's law constants (S_{Hij}) in the ILs at 298.15 K, and the solid filled bars represent the ideal selectivity calculated from the ratio of mass fractions (S_{Wij}) in the ILs at 298.15 K and 1.0 MPa. Data for [C_6C_1im][Cl] reported by Morais et al.[15]

3.7. Fickian Diffusion Coefficients. Diffusion coefficients are another key property used for designing new separation processes. The simplified Fickian diffusion model discussed in Section 2.5 was used to determine diffusion coefficients for HFC-32 and HFC-125 in each IL using the time-dependent absorption data. Table 15 shows the IL viscosities at 0.1 MPa and 298.15 K and diffusion coefficients at 0.05 MPa and 298.15 K for the HFC/IL systems.

According to the Stokes–Einstein equation[54]

$$D = \frac{k_B T}{6\pi\eta R} \quad (28)$$

the diffusion coefficient (D) is inversely proportional to the viscosity (η) and the molecular radius of the solute (R) and proportional to the absolute temperature (T). The viscosity of the IL is also dependent on the amount of refrigerant absorbed (C_s) at the given T and P. Overall, the magnitude of the diffusion coefficients for HFCs in ILs is lower than that of most of the gases in ordinary liquids (e.g., water, alcohols, etc.). In fact, the HFC diffusion coefficients in ILs fall between values expected for gases into liquids (10^{-5} cm^2·s^{-1}) and gases into solids (10^{-9} cm^2·s^{-1}) with similar magnitudes to those found for gases into polymers (10^{-7} cm^2·s^{-1}).[54] One explanation is the relatively high viscosities are due in part to the Coulombic forces between cations and anions. The reported diffusion coefficients are similar to previously reported values by Morais et al. and others.[15] As expected, HFC-32 ($D_{HFC\text{-}32}$ = 2.9 × 10^{-7} cm^2·s^{-1}) and HFC-125 ($D_{HFC\text{-}125}$ = 1.1 − 10^{-7} cm^2·s^{-1}) had the highest diffusion coefficients in [$P_{6,6,6,14}$][Cl], which has the lowest viscosity (1.68 ± 0.25 Pa·s). The molecular radius for HFC-32 (0.18 nm) is approximately 22% smaller than the

https://doi.org/10.1021/acssuschemeng.1c06252
ACS Sustainable Chem. Eng. 2022, 10, 816–830

Table 15. Viscosities for ILs at 0.1 MPa and 298.15 K and Estimated Fickian Diffusion Coefficients for HFC-32/IL and HFC-125/IL Systems at 0.05 MPa and 298.15 K[a,b]

		HFC-32 (1)/IL (2)		HFC-125 (1)/IL (2)	
ionic liquid	viscosity (Pa·s)	D (10^{-7} cm^2·s^{-1})	C_s (wt %)	D (10^{-7} cm^2·s^{-1})	C_s (wt %)
[C_6C_1im][I]	1.8 ± 0.2[20]	0.9	0.5	0.2	0.3
[C_6C_1im][Br]	3.6 ± 0.8[22]	0.6	0.7	0.2	0.7
[C_6C_1im][Cl]	18.1 ± 1.8[15,23]	1.5	0.5	0.4	3.2
[C_4C_1im][Cl]	[c]	0.3	0.8	0.2	0.6
[C_3C_1im][Cl]	[c]	0.4	0.7	0.4	0.3
[C_2C_1im][Cl]	[c]				
[$P_{14,6,6,6}$][Cl]	1.68 ± 0.25[31]	2.9	1.3	1.1	7.8

[a]Estimated uncertainty in diffusivity was estimated to be within a factor of 2. [b]Data for [C_6C_1im][Cl] reported by Morais et al.[15] [c]Solid at 298.15 K.

molecular radius for HFC-125 (0.23 nm), which explains why in most cases the $D_{HFC\text{-}32}$ is larger than the $D_{HFC\text{-}125}$.

4. CONCLUSIONS

HFCs are widely used throughout the refrigeration and air-conditioning industry; however, the high GWPs for some HFCs have resulted in legislation being enacted requiring them to be phased out over the next two decades. Azeotropic refrigerant mixtures, such as R-410A, complicate the separation and recycling of low-GWP refrigerants such as HFC-32. This research is focused on developing IL entrainers for separating HFC-32 and HFC-125 using extractive distillation. VLE data for HFC-32 and HFC-125 are compared for six ILs with three halogen anions ($[I]^-$, $[Br]^-$, and $[Cl]^-$) and two cations (imidazolium $[C_xC_1im]^+$ with alkyl chain lengths of x = 2, 3, 4, and 6, and phosphonium $[P_{6,6,6,14}]^+$) at 298.15 K. The variation of the anion resulted in relatively no change in HFC-32 solubility; however, HFC-125 solubility increased as the size of the anion decreased ($[I]^- > [Br]^- > [Cl]^-$), and the strength of the Lewis basicity and electronegativity of the anion increased. Variation of the alkyl chain length resulted in very little change in HFC-32 solubility. On the other hand, HFC-125 solubility increased with an increase in the alkyl chain length due likely to increases in van der Waals forces. The phosphonium-based IL had higher HFC-32 and HFC-125 solubility at low pressures compared to the imidazolium-based IL with the same chloride anion. Diffusion coefficients for HFC-32 and HFC-125 are lower than those found for gases into ordinary liquids and similar to those for gas-polymer systems due to higher IL viscosities. The larger diffusion coefficients for HFC-32 versus HFC-125 in ILs agree with the smaller molecular size for HFC-32. Selectivities based on Henry's law constants and the mass ratio indicate that [C_6C_1im][Cl] and [$P_{6,6,6,14}$][Cl] are the most promising candidates as entrainers for the separation of R-410A using extractive distillation.

ASSOCIATED CONTENT

Supporting Information

The Supporting Information is available free of charge at https://pubs.acs.org/doi/10.1021/acssuschemeng.1c06252.

VLE data comparison for [C_4C_1im][PF_6] at 298.15 K; composition and GWP of common HFC refrigerants; covariance matrices for the PR EOS-fitted parameters; and high-pressure view cell and phase change data (PDF)

AUTHOR INFORMATION

Corresponding Author

Mark B. Shiflett − *Department of Chemical & Petroleum Engineering, University of Kansas, Lawrence, Kansas 66045, United States; Institute for Sustainable Engineering, University of Kansas, Lawrence, Kansas 66045, United States;* orcid.org/0000-0002-8934-6192; Email: mark.b.shiflett@ku.edu

Authors

Kalin R. Baca − *Department of Chemical & Petroleum Engineering, University of Kansas, Lawrence, Kansas 66045, United States; Institute for Sustainable Engineering, University of Kansas, Lawrence, Kansas 66045, United States;* orcid.org/0000-0002-7292-8698

Greta M. Olsen − *Department of Chemical & Petroleum Engineering, University of Kansas, Lawrence, Kansas 66045, United States; Institute for Sustainable Engineering, University of Kansas, Lawrence, Kansas 66045, United States;* orcid.org/0000-0003-1415-5153

Lucia Matamoros Valenciano − *Department of Chemical & Petroleum Engineering, University of Kansas, Lawrence, Kansas 66045, United States; Institute for Sustainable Engineering, University of Kansas, Lawrence, Kansas 66045, United States;* orcid.org/0000-0002-4964-9148

Madelyn G. Bennett − *Department of Chemical & Petroleum Engineering, University of Kansas, Lawrence, Kansas 66045, United States; Institute for Sustainable Engineering, University of Kansas, Lawrence, Kansas 66045, United States;* orcid.org/0000-0002-0698-7518

Dorothy M. Haggard − *Department of Chemical & Petroleum Engineering, University of Kansas, Lawrence, Kansas 66045, United States; Institute for Sustainable Engineering, University of Kansas, Lawrence, Kansas 66045, United States;* orcid.org/0000-0001-5575-1651

Bridgette J. Befort − *Department of Chemical & Biomolecular Engineering, University of Notre Dame, Notre Dame, Indiana 46556, United States;* orcid.org/0000-0002-2340-6092

Alejandro Garciadiego − *Department of Chemical & Biomolecular Engineering, University of Notre Dame, Notre Dame, Indiana 46556, United States;* orcid.org/0000-0003-0097-3307

Alexander W. Dowling − *Department of Chemical & Biomolecular Engineering, University of Notre Dame, Notre Dame, Indiana 46556, United States;* orcid.org/0000-0001-9383-7499

Edward J. Maginn − *Department of Chemical & Biomolecular Engineering, University of Notre Dame, Notre Dame, Indiana 46556, United States*; orcid.org/0000-0002-6309-1347

Complete contact information is available at: https://pubs.acs.org/10.1021/acssuschemeng.1c06252

Funding

This research was supported by the National Science Foundation under grants no. CBET-1917480 (University of Kansas), CBET-1917474 (University of Notre Dame), and EFMA-2029354 (University of Kansas, University of Notre Dame, Texas A&M University, and Rutgers University).

Notes

The authors declare no competing financial interest.

ACKNOWLEDGMENTS

The authors acknowledge The Chemours Company for providing the HFC-32 and HFC-125 refrigerants for this study, IoLiTec for providing the ionic liquids, and The Wonderful Company for their financial gift.

ABBREVIATIONS

ODP, ozone depletion potential
GWP, global warming potential
IL, ionic liquid
HFC, hydrofluorocarbon
HFO, hydrofluoroolefin
HCFC, hydrochlorofluorocarbon
CFC, chlorofluorocarbon
HFC-125, pentafluoroethane, CHF_2CF_3
HFC-32, difluoromethane, CH_2F_2
$[C_6C_1im][I]$, 1-*n*-hexyl-3-methylimidazolium iodide
$[C_6C_1im][Br]$, 1-*n*-hexyl-3-methylimidazolium bromide
$[C_6C_1im][Cl]$, 1-*n*-hexyl-3-methylimidazolium chloride
$[C_4C_1im][Cl]$, 1-*n*-butyl-3-methylimidazolium chloride
$[C_3C_1im][Cl]$, 1-methyl-3-propylimidazolium chloride
$[C_2C_1im][Cl]$, 1-ethyl-3-methylimidazolium chloride
$[P_{6,6,6,14}][Cl]$, trihexyl(tetradecyl)phosphonium chloride
S_{Hij}, selectivity based on Henry's law constants in the ILs
S_{Wij}, selectivity based on the ratio of the mass fraction in the ILs at 298.15 K and 1 MPa
$D_{HFC\text{-}32}$, diffusion coefficient for HFC-32 in the ILs
$D_{HFC\text{-}125}$, diffusion coefficient for HFC-125 in the ILs
PR EOS, Peng−Robinson equation of state

REFERENCES

(1) Booten, C.; Nicholson, S.; Mann, M.; Abdelaziz, O. *Refrigerants: Market Trends and Supply Chain Assessment*; NREL, 2020.

(2) Process Cooling. Reducing the Environmental Footprint of Your Refrigeration Systems and Chillers | 2016-10-01. https://www.process-cooling.com/articles/88647-reducing-the-environmental-footprint-of-your-refrigeration-systems-and-chillers (accessed Aug 06, 2021).

(3) Asensio-Delgado, S.; Pardo, F.; Zarca, G.; Urtiaga, A. Enhanced Absorption Separation of Hydrofluorocarbon/Hydrofluoroolefin Refrigerant Blends Using Ionic Liquids. *Sep. Purif. Technol.* 2020, *249*, 117136.

(4) Arora, P.; Seshadri, G.; Tyagi, A. K. Fourth-Generation Refrigerant:HFO 1234yf. *Curr. Sci.* 2018, *115*, 1497−1503.

(5) US EPA. Proposed Rule Phasedown of Hydrofluorocarbons: Establishing the Allowance Allocation and Trading Program under the AIM Act. https://www.epa.gov/climate-hfcs-reduction/proposed-rule-phasedown-hydrofluorocarbons-establishing-allowance-allocation (accessed Aug 03, 2021).

(6) US EPA. AIM Act. https://www.epa.gov/climate-hfcs-reduction/aim-act (accessed Aug 06, 2021).

(7) European Environment Agency. Hydrofluorocarbon Phase-Down in Europe. https://www.eea.europa.eu/data-and-maps/indicators/emissions-and-consumption-of-fluorinated-3 (accessed Sept 11, 2021).

(8) Pardo, F.; Zarca, G.; Urtiaga, A. Effect of Feed Pressure and Long-Term Separation Performance of Pebax-Ionic Liquid Membranes for the Recovery of Difluoromethane (R32) from Refrigerant Mixture R410A. *J. Membr. Sci.* 2021, *618*, 118744.

(9) Myhre, G.; Shindell, D.; Bréon, F.-M.; Collins, W.; Fuglestvedt, J.; Huang, J.; Koch, D.; Lamarque, J.-F.; Lee, D.; Mendoza, B.; Nakajima, T.; Robock, A.; Stephens, G.; Takemura, T.; Zhang, H. 2013: Anthropogenic and Natural Radiative Forcing. In *Climate Change 2013: The Physical Science Basis. Contribution of Working Group I to the Fifth Assessment Report of the Intergovernmental Panel on Climate Change*; Stocker, T. F., Qin, D., Plattner, G.-K., Tignor, M., Allen, S. K., Boschung, J., Nauels, A., Xia, Y., Bex, V., Midgley, P. M., Eds.; Cambridge University Press: Cambridge, United Kingdom and New York, NY, USA, 2013; pp 731−737.

(10) *2018 Assessment Report of the Refrigeration*, Air Conditioning and Heat Pumps Technical Options Committee; 2019.

(11) Zhang, Z.; Zhang, Z.; Dong, B.; Chen, J.; Xin, H.; Zhang, Q. Vapor-Liquid Equilibrium Experiment and Model Prediction for Separating Ethyl Propionate and Ethanol Using Ionic Liquids with Acetate Anion. *J. Mol. Liq.* 2020, *318*, 113688.

(12) Li, H.; Sun, G.; Li, D.; Xi, L.; Zhou, P.; Li, X.; Zhang, J.; Gao, X. Molecular Interaction Mechanism in the Separation of a Binary Azeotropic System by Extractive Distillation with Ionic Liquid. *Green Energy Environ.* 2021, *6*, 329−338.

(13) Zhu, Z.; Li, H.; Xu, Y.; Zhang, W.; Shen, Y.; Gao, J.; Wang, L.; Wang, Y. Quantum Chemical Calculation, Molecular Dynamics Simulation and Process Design for Separation of Heptane - Butanol Using Ionic Liquids Extraction. *J. Mol. Liq.* 2020, *316*, 113851.

(14) Zhang, W.; Chen, Z.; Shen, Y.; Li, G.; Dai, Y.; Qi, J.; Ma, Y.; Yang, S.; Wang, Y. Molecular Mechanism and Extraction Performance Evaluation for Separation of Methanol and N-Hexane via Ionic Liquids as Extractant. *ACS Sustainable Chem. Eng.* 2020, *8*, 8700−8712.

(15) Morais, A. R. C.; Harders, A. N.; Baca, K. R.; Olsen, G. M.; Befort, B. J.; Dowling, A. W.; Maginn, E. J.; Shiflett, M. B. Phase Equilibria, Diffusivities, and Equation of State Modeling of HFC-32 and HFC-125 in Imidazolium-Based Ionic Liquids for the Separation of R-410A. *Ind. Eng. Chem. Res.* 2020, *59*, 18222−18235.

(16) Lemmon, E. W.; Bell, I. H.; Huber, M. L.; McLinden, M. O. *NIST Standard Reference Database 23: Reference Fluid Thermodynamic and Transport Properties-REFPROP*, Version 10.0, National Institute of Standards and Technology, Standard Reference Data Program. Gaithersburg 2018.

(17) Dong, Q.; Muzny, C. D.; Kazakov, A.; Diky, V.; Magee, J. W.; Widegren, J. A.; Chirico, R. D.; Marsh, K. N.; Frenkel, M. ILThermo: A Free-Access Web Database for Thermodynamic Properties of Ionic Liquids. *J. Chem. Eng. Data* 2007, *52*, 1151−1159.

(18) Kazakov, A. F.; Magee, J. W.; Chirico, R. D.; Diky, V.; Kroenlein, K. G.; Muzny, C. D.; Frenkel, M. D. *Ionic Liquids Database ILThermo* (v2.0); NIST, 2013.

(19) Součková, M.; Klomfar, J.; Pátek, J. Surface Tension and 0.1 MPa Density Data for 1- C n-3-Methylimidazolium Iodides with n = 3, 4, and 6, Validated Using a Parachor and Group Contribution Model. *J. Chem. Thermodyn.* 2015, *83*, 52−60.

(20) Ghatee, M. H.; Zare, M.; Moosavi, F.; Zolghadr, A. R. Temperature-Dependent Density and Viscosity of the Ionic Liquids 1-Alkyl-3-Methylimidazolium Iodides: Experiment and Molecular Dynamics Simulation. *J. Chem. Eng. Data* 2010, *55*, 3084−3088.

(21) Klomfar, J.; Součková, M.; Pátek, J. Experimental Densities and Surface Tension and Models Generating the Best-Current-Knowledge Values of Them for Members of 1-Cn-3-Methylimidazolium Bromide Homologous Series. *J. Chem. Thermodyn.* 2018, *118*, 225−234.

(22) Li, J.-G.; Hu, Y.-F.; Sun, S.-F.; Liu, Y.-S.; Liu, Z.-C. Densities and dynamic viscosities of the binary system (water+1-hexyl-3-methylimidazolium bromide) at different temperatures. *J. Chem. Thermodyn.* 2010, *42*, 904−908.
(23) Gómez, E.; González, B.; Domínguez, A.; Tojo, E.; Tojo, J. Dynamic Viscosities of a Series of 1-Alkyl-3-Methylimidazolium Chloride Ionic Liquids and Their Binary Mixtures with Water at Several Temperatures. *J. Chem. Eng. Data* 2006, *51*, 696−701.
(24) *Technical Data Sheet: 1-Butyl-3-Methylimidazolium Chloride*, 2015.
(25) *Safety Data Sheet: 1-Butyl-3-Methylimidazolium Chloride*, 2019.
(26) Govinda, V.; Attri, P.; Venkatesu, P.; Venkateswarlu, P. Thermophysical Properties of Dimethylsulfoxide with Ionic Liquids at Various Temperatures. *Fluid Phase Equilib.* 2011, *304*, 35−43.
(27) *Technical Data Sheet: 1-Methyl-3-Propylimidazolium Chloride*, 2016.
(28) Součková, M.; Klomfar, J.; Pátek, J. Group contribution and parachor analysis of experimental data on density and surface tension for members of the homologous series of 1-C -3-methylimidazolium chlorides. *Fluid Phase Equilib.* 2017, *454*, 43−56.
(29) *Safety Data Sheet: 1-Ethyl-3-Methylimidazolium Chloride*, 2021.
(30) *Technical Data Sheet: 1-Ethyl-3-Methylimidazolium Chloride*, 2017.
(31) McAtee, Z. P.; Heitz, M. P. Density, Viscosity and Excess Properties in the Trihexyltetradecylphosphonium Chloride Ionic Liquid/Methanol Cosolvent System. *J. Chem. Therm.* 2016, *93*, 34−44.
(32) Minnick, D. L.; Turnaoglu, T.; Rocha, M. A.; Shiflett, M. B. Review Article: Gas and Vapor Sorption Measurements Using Electronic Beam Balances. *J. Vac. Sci. Technol., A* 2018, *36*, 050801.
(33) Sousa, J. M. M. V.; Granjo, J. F. O.; Queimada, A. J.; Ferreira, A. G. M.; Oliveira, N. M. C.; Fonseca, I. M. A. Solubility of Hydrofluorocarbons in Phosphonium-Based Ionic Liquids: Experimental and Modelling Study. *J. Chem. Therm.* 2014, *79*, 184−191.
(34) Shiflett, M. B.; Harmer, M. A.; Junk, C. P.; Yokozeki, A. Solubility and Diffusivity of 1,1,1,2-Tetrafluoroethane in Room-Temperature Ionic Liquids. *Fluid Phase Equilib.* 2006, *242*, 220−232.
(35) Shiflett, M. B.; Yokozeki, A. Solubilities and Diffusivities of Carbon Dioxide in Ionic Liquids: [Bmim][PF6] and [Bmim][BF4]. *Ind. Eng. Chem. Res.* 2005, *44*, 4453−4464.
(36) Yokozeki, A.; Shiflett, M. B. Global phase behaviors of trifluoromethane in ionic liquid [bmim][PF6]. *AIChE J.* 2006, *52*, 3952−3957.
(37) Yokozeki, A.; Shiflett, M. B. Vapor-liquid equilibria of ammonia +ionic liquid mixtures. *Appl. Energy* 2007, *84*, 1258−1273.
(38) Shiflett, M. B.; Yokozeki, A. Solubility and Diffusivity of Hydrofluorocarbons in Room-Temperature Ionic Liquids. *AIChE J.* 2006, *52*, 1205−1219.
(39) Minnick, D. L.; Shiflett, M. B. Solubility and Diffusivity of Chlorodifluoromethane in Imidazolium Ionic Liquids: [Emim][Tf2N], [Bmim][BF4], [Bmim][PF6], and [Emim][TFES]. *Ind. Eng. Chem. Res.* 2019, *58*, 11072−11081.
(40) Shojaeian, A.; Fatoorehchi, H. Modeling Solubility of Refrigerants in Ionic Liquids Using Peng Robinson-Two State Equation of State. *Fluid Phase Equilib.* 2019, *486*, 80−90.
(41) Orbey, H.; Sandler, S. I. Equation of State Modeling of Refrigerant Mixtures. *Ind. Eng. Chem. Res.* 2002, *34*, 2520−2525.
(42) Teodorescu, M.; Lugo, L.; Fernández, J. Modeling of Gas Solubility Data for HFCs−Lubricant Oil Binary Systems by Means of the SRK Equation of State. *Int. J. Thermophys.* 2003, *24*, 1043−1060.
(43) Ren, W.; Sensenich, B.; Scurto, A. M. High-pressure phase equilibria of {carbon dioxide (CO2)+n-alkyl-imidazolium bis-(trifluoromethylsulfonyl)amide} ionic liquids. *J. Chem. Therm.* 2010, *42*, 305−311.
(44) Yokozeki, A.; Shiflett, M. B. Gas Solubilities in Ionic Liquids Using a Generic van Der Waals Equation of State. *J. Supercrit. Fluids* 2010, *55*, 846−851.
(45) Lee, A.; Ghouse, J. H.; Eslick, J. C.; Laird, C. D.; Siirola, J. D.; Zamarripa, M. A.; Gunter, D.; Shinn, J. H.; Dowling, A. W.; Bhattacharyya, D.; Biegler, L. T.; Burgard, A. P.; Miller, D. C. The IDAES process modeling framework and model library-Flexibility for process simulation and optimization. *J. Adv. Manuf. Process.* 2021, *3*, No. e10095.
(46) Reid, R. C.; Prausnitz, J. M.; Poling, B. E. *The Properties of Gases and Liquids*; McGraw-Hill Professional Publishing, 1987; pp 95−149.
(47) Rebelo, L. P. N.; Canongia Lopes, J. N.; Esperança, J. M. S. S.; Filipe, E. On the Critical Temperature, Normal Boiling Point, and Vapor Pressure of Ionic Liquids. *J. Phys. Chem. B* 2005, *109*, 6040−6043.
(48) Rai, N.; Maginn, E. J. Critical behaviour and vapour-liquid coexistence of 1-alkyl-3-methylimidazolium bis-(trifluoromethylsulfonyl)amide ionic liquidsvia Monte Carlo simulations. *Faraday Discuss.* 2011, *154*, 53−69.
(49) Yokozeki, A. Solubility of Refrigerants in Various Lubricants. *Int. J. Thermophys.* 2001, *22*, 1057−1071.
(50) Sander, R.; Acree, W. E.; de Visscher, A.; Schwartz, S. E.; Wallington, T. Henry's Law Constants. *Pure Appl. Chem.* 2020, *92*, 1.
(51) Lozano-Martín, D.; Inês Cardoso Vieira, S.; Paredes, X.; Vitoriano Lourenço, M. J.; Nieto de Castro, C. A.; Sengers, J. v.; Massonne, K. Thermal Conductivity of Metastable Ionic Liquid [C2mim][CH3SO3]. *Molecules* 2020, *25*, 4290.
(52) Angell, C. A. On the Importance of the Metastable Liquid State and Glass Transition Phenomenon to Transport and Structure Studies in Ionic Liquids. I. Transport Properties1. *J. Phys. Chem.* 1966, *70*, 2793−2803.
(53) Vila, J.; Fernández-Castro, B.; Rilo, E.; Carrete, J.; Domínguez-Pérez, M.; Rodríguez, J. R.; García, M.; Varela, L. M.; Cabeza, O. Liquid-solid-liquid phase transition hysteresis loops in the ionic conductivity of ten imidazolium-based ionic liquids. *Fluid Phase Equilib.* 2012, *320*, 1−10.
(54) Cussler, E. L. Diffusion. *Mass Transfer in Fluid Systems*, 3rd ed.; Cambridge University Press: Cambridge, 2009.

https://doi.org/10.1021/acssuschemeng.1c06252
ACS Sustainable Chem. Eng. 2022, 10, 816−830